arXiv:1512.07769v3 [astro-ph.CO] 3 May 2016

Inflation model constraints from data released in 2015

Qing-Guo Huang *, Ke Wang † and Sai Wang ‡

Key Laboratory of Theoretical Physics,

Institute of Theoretical Physics, Chinese Academy of Sciences,

Beijing 100190, People's Republic of China

(Dated: March 6, 2022)

We provide the latest constraints on the power spectra of both scalar and tensor perturbations from the CMB data (including *Planck* 2015, BICEP2 & *Keck Array* experiments) and the new BAO scales from SDSS-III BOSS observation. We find that the inflation model with a convex potential is not favored and both the inflation model with a monomial potential and the natural inflation model are marginally disfavored at around 95% confidence level. But both the Brane inflation model and the Starobinsky inflation model fit the data quite well.

* huangqg@itp.ac.cn

† wangke@itp.ac.cn

‡ wangsai@itp.ac.cn

I. INTRODUCTION

In the past three decades, the inflation model [1–4] was taken as the standard paradigm of the very early Universe. It not only resolves the flatness, horizon and monopole problems in the hot big bang model, but also generates the primordial density perturbations seeding the anisotropies in the cosmic microwave background (CMB) and the large-scale structure in our Universe. The simple inflation model predicts that the power spectra of both primordial scalar and tensor perturbations are adiabatic, Gaussian and nearly scale-invariant. In particular, the amplitude of primordial tensor perturbations is determined by the energy scale of inflation. Actually the primordial perturbations contribute to the anisotropies and polarizations of CMB as well as CMB lensing, which can be precisely measured by the ground-based or satellite CMB experiments, for example the *Planck* satellite [5, 6]. Therefore one can estimate the cosmological parameters and explore the nature of inflation by using the CMB data.

The excess of B-mode power over the base lensed-ΛCDM expectation detected by BICEP2 [7] can be explained by the polarized thermal dust, not the primordial gravitational waves [8, 9]. Subtracting the contributions to the CMB B-mode from Galactic polarized dust measured by Planck collaboration in [10], the tensor-to-scalar ratio $r \lesssim 0.1$ at 95% confidence level (C.L.) was obtained in [11] which was confirmed by a joint analysis of B-mode polarization data of BICEP2/Keck Array and *Planck* (BKP) in [12]. Furthermore, because of the tight constraint on the tensor-to-scalar ratio, the chaotic inflation model with a potential $V(\phi) \propto \phi^2$ was disfavored at more than 2σ C.L. in [11]. All of these results are confirmed by the *Planck* 2015 results [6] in which the scalar spectral index $n_s = 0.968 \pm 0.006$ at 68% C.L. and the tensor-to-scalar ratio $r_{0.002} < 0.11$ at 95% C.L. by fitting the *Planck* TT,TE,EE+lowP+lensing combination (P15).

Recently BICEP2 & *Keck Array* CMB polarization experiments released the B-mode polarization data up to and including the 2014 observing season in [13]. This dataset includes the first *Keck Array* B-mode data at 95 GHz. The BICEP2 & *Keck Array* B-mode data (BK14) implies $r_{0.05} < 0.09$ (95% C.L.). Combining with *Planck* 2015 TT+lowP+lensing and some other external data, the upper bound on r becomes $r_{0.05} < 0.07$ (95% C.L.) [13] in the base ΛCDM+r model. This constraint on r is the strongest one to date, even though it is model-dependent in some sense.

In addition, the Baryon Acoustic Oscillation (BAO) data can significantly break the degeneracies between cosmological parameters. Recently, the BAO distance scale measurements were updated via an anisotropic analysis of BAO scale in the correlation function [14] and power spectrum [15] of the CMASS and LOWZ galaxy samples from Data Release 12 of the SDSS-III Baryon Oscillation Spectroscopic Survey (BOSS DR12). The total volume probed in DR12 has a 10% increment from DR11 and the experimental uncertainty has been reduced. In this paper, the BAO data we will adopt include 6dFGS [16], MGS [17], BOSS DR12 CMASS [15] and LOWZ [15] (BAO15).

In this paper we will make a joint analysis of the recently released CMB and BAO data to constrain the cosmological parameters and the inflation models. Our paper is arranged as follows. In Sec. II, we constrain the power spectra of both scalar and tensor perturbations by using the data combination of P15+BK14+BAO15. In Sec. III, we will test several inflation models in two different methods. The summary and discussion are included in Sec. IV.

II. CONSTRAINTS ON THE POWER SPECTRA OF SCALAR AND TENSOR PERTURBATIONS

In this section, we will make a joint analysis of P15+BK14+BAO15 dataset to constrain the cosmological parameters in the base ΛCDM+r model and the other two extended models.

In general, the power spectra of primordial scalar and tensor perturbations can be parameterized as follows

$$P_s(k) = A_s \left(\frac{k}{k_p}\right)^{n_s-1+\frac{1}{2}\frac{dn_s}{d\ln k}\left(\ln\frac{k}{k_p}\right)+\frac{1}{6}\frac{d^2n_s}{d\ln k^2}\left(\ln\frac{k}{k_p}\right)^2}, \quad (1)$$

$$P_t(k) = A_t \left(\frac{k}{k_p}\right)^{n_t}, \quad (2)$$

where A_s and A_t denote the amplitudes of scalar and tensor power spectra at the pivot scale k_p, n_s and n_t denote the spectral indices of scalar and tensor power spectra, $n_{\rm run} \equiv dn_s/d\ln k$ and $n_{\rm run,run} \equiv d^2n_s/d\ln k^2$ denote the running and the running of running of scalar spectral index. In this paper, we set the pivot scale as $k_p = 0.01$ Mpc^{-1}. The spectral index of tensor power spectrum is set as $n_t = -A_t/(8A_s)$ which is the consistency relation for the canonical single-field slow-roll inflation model [18]. In principle, n_t can be taken as a free parameter. However, n_t cannot be well constrained by the current observations [19–21], even though

$n_t \simeq 0$ is consistent with the current datasets. The measurement on n_t is expected to be improved by some forthcoming experiments [22].

In this paper we consider three cosmological models. The first one is the base ΛCDM+r model in which there are seven free parameters: the baryon density today ($\Omega_b h^2$), the cold dark matter density today ($\Omega_c h^2$), the $100\times$ angular scale of the sound horizon at last-scattering ($100\theta_{\rm MC}$), the Thomson scattering optical depth due to the reionization (τ), the amplitude of scalar power spectrum (A_s), the spectral index of scalar power spectrum (n_s) and the tensor-to-scalar ratio (r). The second one is the base ΛCDM+r+nrun model where the running of scalar spectral index ($dn_s/d\ln k$) is included as an additional free parameter. The third one is the base ΛCDM+r+nrun+nrunrun model in which an additional parameter, namely the running of running ($d^2n_s/d\ln k^2$), is added.

The BAO data and 1σ uncertainty of BOSS DR12 LOWZ and CMASS samples are listed in Tab. I. Their consensus values are listed here, which are used in this paper. Here z_{eff}

z_{eff}	BOSS DR12	$H(z_{eff})r_d[10^3{\rm km}\cdot s^{-1}]$	$D_A(z_{eff})/r_d$	$\rho_{D_A,H}$
0.32	LOWZ	11.64 ± 0.70	6.76 ± 0.15	0.35
0.57	CMASS	14.66 ± 0.42	9.47 ± 0.13	0.54

TABLE I: The distance measurement from the anisotropic analysis of BAO scale in the CMASS and LOWZ galaxy samples released by SDSS-III BOSS DR12 [15].

denotes the effective redshift for CMASS and LOWZ samples, respectively. $H(z_{eff})$ and $D_A(z_{eff})$ are Hubble parameter and angular diameter distance at redshift z_{eff}, respectively. r_d denotes the comoving sound horizon at the redshift of baryon drag epoch. In addition, $\rho_{D_A,H}$ is the normalized correlation between $D_A(z_{eff})$ and $H(z_{eff})$.

We can add a likelihood of the above BAO scales into our data analysis. The likelihood is given by

$$-2\ln\mathcal{L} = \sum_{k=1}^{2}\left(D^{data}-D^{model}\right)_k^T C_k^{-1}\left(D^{data}-D^{model}\right)_k \ , \tag{3}$$

where $k=1$ for LOWZ and $k=2$ for CMASS. We denote $D_k^{data} \equiv (Hr_d, D_A r_d)_k^T$ for the observational BAO data in Tab. I. Calculated by CAMB [23, 24], D_k^{model} denote the corresponding theoretical predictions of cosmological models. We denote C_k as the covariance

matrix, namely

$$C_k = \begin{pmatrix} \sigma^2_{D_A} & \rho_{D_A,H}\sigma_{D_A}\sigma_H \\ \rho_{D_A,H}\sigma_{D_A}\sigma_H & \sigma^2_H \end{pmatrix}_k \tag{4}$$

where σ_{D_A} and σ_H respectively denote 1σ uncertainty of Hr_d and $D_A r_d$ in Tab. I.

In this paper, we use the Markov Chain Monte Carlo sampler (CosmoMC) [25] to explore the space of cosmological parameters in each cosmological model. Our results are summarized in Tab. II, in which we list the constraints on all of the cosmological parameters as well as the best-fit χ^2 for these three cosmological models.

Parameters	ΛCDM+r	ΛCDM+r+nrun	ΛCDM+r+nrun+nrunrun
$\Omega_b h^2$	0.02227 ± 0.00014	0.02230 ± 0.00015	0.02223 ± 0.00015
$\Omega_c h^2$	0.1188 ± 0.0010	0.1188 ± 0.0010	0.1190 ± 0.0010
$100\theta_{MC}$	1.04091 ± 0.00030	1.04091 ± 0.00030	1.04092 ± 0.00029
τ	0.067 ± 0.012	0.067 ± 0.012	0.072 ± 0.013
$\ln(10^{10} A_s)$	3.119 ± 0.021	3.117 ± 0.021	3.132 ± 0.023
n_s	0.9669 ± 0.0040	0.9721 ± 0.0108	0.9756 ± 0.0111
$r_{0.01}$ (95% C.L.)	< 0.0685	< 0.0751	< 0.0814
$dn_s/d\ln k$	-	-0.0035 ± 0.0068	-0.0247 ± 0.0148
$d^2 n_s/d\ln k^2$	-	-	0.0211 ± 0.0130
χ^2	13608.6	13608.6	13605.3

TABLE II: The 68% limits on the cosmological parameters in three cosmological models from P15+BK14+BAO15 data combination.

The marginalized contour plots and the likelihood distributions of r and n_s in the base ΛCDM+r model are depicted in Fig. 1. The constraints on r and n_s are given by

$$r_{0.01} < 0.0685 \ \ (95\% \text{ C.L.}) \ , \tag{5}$$

$$n_s = 0.9669 \pm 0.0040 \ \ (68\% \text{ C.L.}) \ . \tag{6}$$

The primordial scalar power spectrum deviates from the Harrison-Zel'dovich spectrum at more than 8σ C.L..

The marginalized contour plots and the likelihood distributions of r, n_s and $dn_s/d\ln k$ in the base ΛCDM+r+nrun model show up in Fig. 2. We see that the constraints on r, n_s

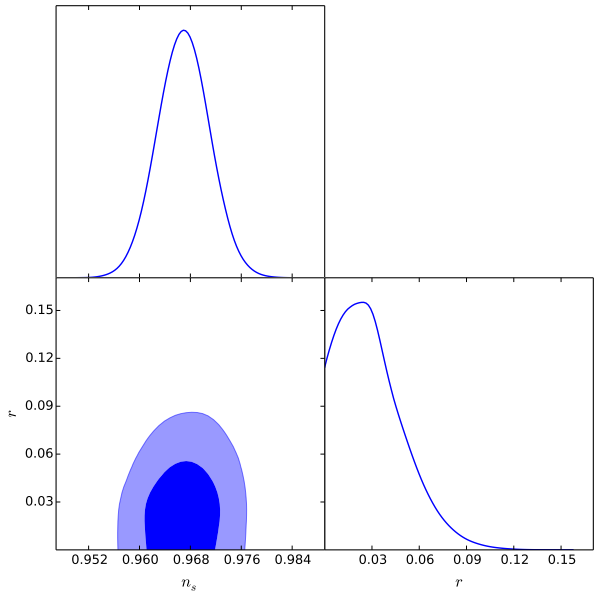


FIG. 1: The marginalized contour plots and the likelihood distributions of r and n_s in the base ΛCDM+r model.

and $dn_s/d\ln k$ read

$$r_{0.01} < 0.0751 \quad (95\%\ \text{C.L.})\ , \tag{7}$$

$$n_s = 0.9721 \pm 0.0108 \quad (68\%\ \text{C.L.})\ , \tag{8}$$

$$dn_s/d\ln k = -0.0035 \pm 0.0068 \quad (68\%\ \text{C.L.})\ . \tag{9}$$

Even though there is one more parameter in the ΛCDM+r+nrun model, the best-fit χ^2 is the same as that in the ΛCDM+r model. We conclude that P15+BK14+BAO15 data do not prefer a non-zero running of scalar spectral index from the statistic point of view.

Finally, the marginalized contour plots and the likelihood distributions of r, n_s, $dn_s/d\ln k$ and $d^2n_s/d\ln k^2$ in the base ΛCDM+r+nrun+nrunrun model are illustrated in Fig. 3. We see that the constraints on r, n_s, $dn_s/d\ln k$ and $d^2n_s/d\ln k^2$ are

$$r_{0.01} < 0.0814 \quad (95\%\ \text{C.L.})\ , \tag{10}$$

$$n_s = 0.9756 \pm 0.0111 \quad (68\%\ \text{C.L.})\ , \tag{11}$$

$$dn_s/d\ln k = -0.0247 \pm 0.0148 \quad (68\%\ \text{C.L.})\ , \tag{12}$$

$$d^2n_s/d\ln k^2 = 0.0211 \pm 0.0130 \quad (68\%\ \text{C.L.})\ . \tag{13}$$

Our results show a slight preference for the negative running and a positive running of

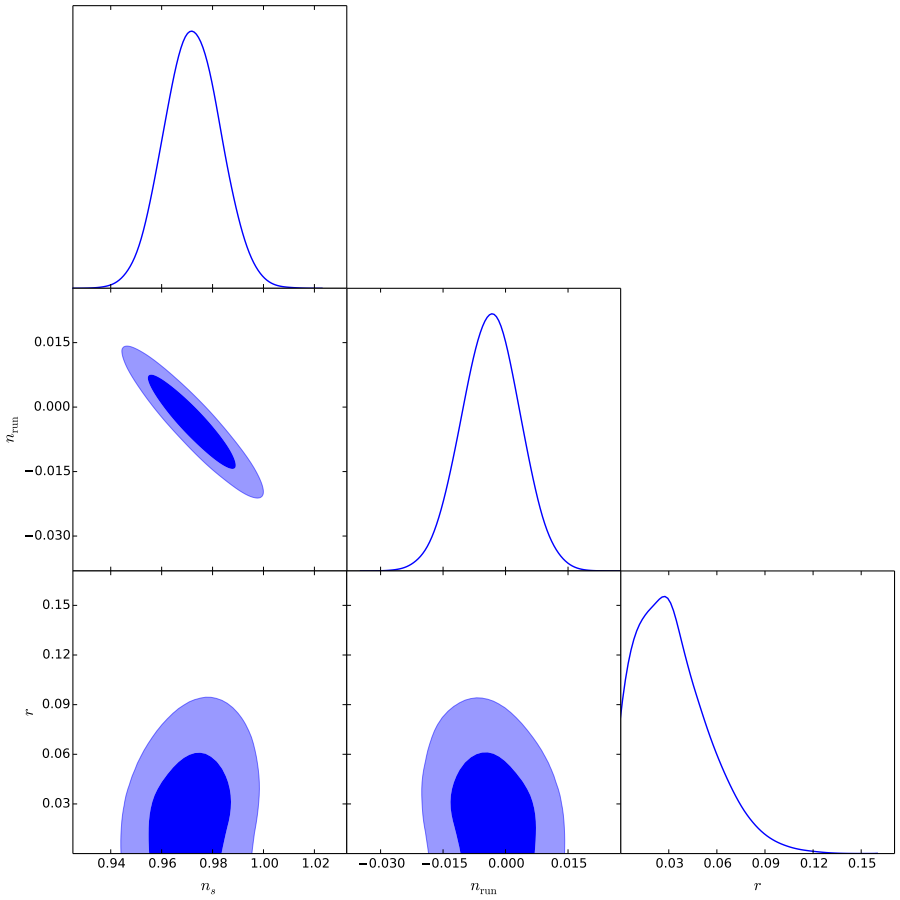


FIG. 2: The marginalized contour plots and the likelihood distributions of r, n_s and $n_{\rm run} \equiv dn_s/d\ln k$ in the base ΛCDM+r+nrun model.

running of the scalar spectral index at the pivot scale $k_p = 0.01$ Mpc^{-1}, and $\Delta\chi^2 \simeq -3.3$ compared to the base ΛCDM+r model.

III. CONSTRAINTS ON INFLATION

The equations of motion for the canonical single-field slow-roll inflation take the form

$$H^2 = \frac{1}{3M_p^2}\left[\frac{1}{2}\dot{\phi}^2 + V(\phi)\right], \tag{14}$$

$$\ddot{\phi} + 3H\dot{\phi} + V'(\phi) = 0, \tag{15}$$

where $M_p = 1/\sqrt{8\pi G}$ is the reduced Planck energy scale, the dot and prime denote the derivative with respect to the cosmic time t and the inflaton field ϕ, respectively. The

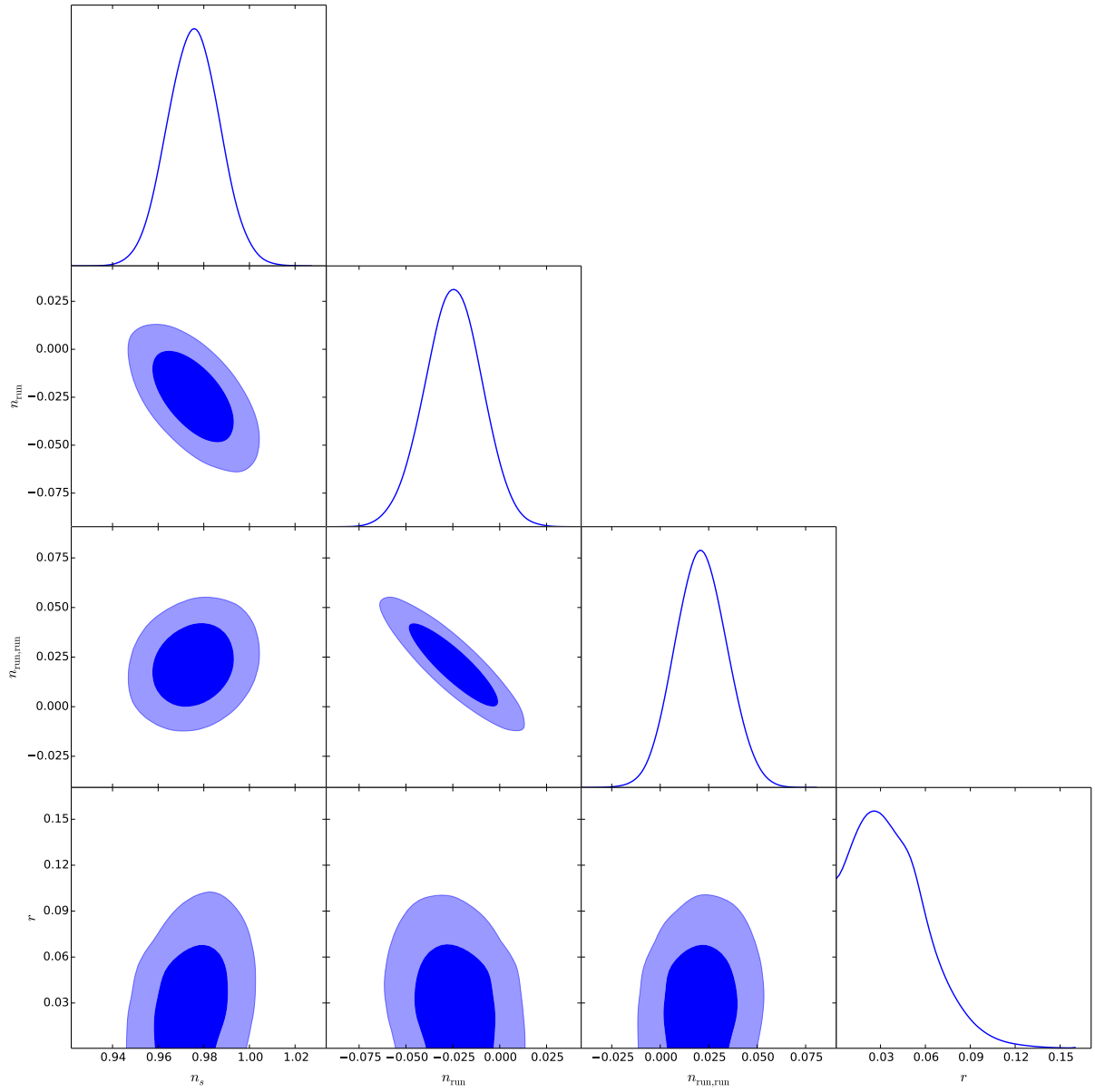


FIG. 3: The marginalized contour plots and the likelihood distributions of r, n_s, $n_{\rm run} \equiv dn_s/d\ln k$ and $n_{\rm run,run} \equiv d^2n_s/d\ln k^2$ in the base ΛCDM+r+nrun+nrunrun model.

inflaton field slowly rolls down its potential if $\epsilon \ll 1$ and $|\eta| \ll 1$, where

$$\epsilon \equiv \frac{M_p^2}{2}\left(\frac{V'}{V}\right)^2, \tag{16}$$

$$\eta \equiv M_p^2\frac{V''}{V}. \tag{17}$$

In this limit, the equations of motion are simplified to

$$H^2 \simeq \frac{V(\phi)}{3M_p^2}, \tag{18}$$

$$3H\dot{\phi} \simeq -V'(\phi). \tag{19}$$

From the dynamics of inflation, we have

$$\eta = 2\epsilon + \frac{1}{2}\frac{d\ln\epsilon}{dN}, \tag{20}$$

where $N \equiv \int_t^{t_{\rm end}} H(t')dt'$ is the number of e-folds before the end of inflation. The amplitudes of scalar and tensor power spectra are respectively given by

$$P_s = \frac{V}{24\pi^2 M_p^2 \epsilon}, \tag{21}$$

$$P_t = \frac{2V}{3\pi^2 M_p^2}. \tag{22}$$

Therefore the tensor-to-scalar ratio and the spectral index of scalar power spectrum are related to the slow-roll parameters by

$$r = 16\epsilon, \tag{23}$$

$$n_s = 1 - 6\epsilon + 2\eta. \tag{24}$$

See, for example, [26] in detail.

A. Selection of inflation models

There are a large number of inflation models in the market [27]. It is almost impossible to figure out a unique inflation model even when the cosmological parameters are measured very accurately, because the number of the cosmological parameters we can measure should be limited. In general, the simplicity is considered as a basic principle we should follow. In this subsection, we only take into account a few simple inflation models and compare them with the global fitting results given in the former section. Our main results are illustrated in Fig. 4. At first glance, we see that the inflation model with a concave potential is preferred at around 95% C.L..

The inflation model with a monomial potential $V(\phi) \sim \phi^n$ [28] is the simplest class of inflation models, and is the prototype of chaotic inflation model. The predictions of this

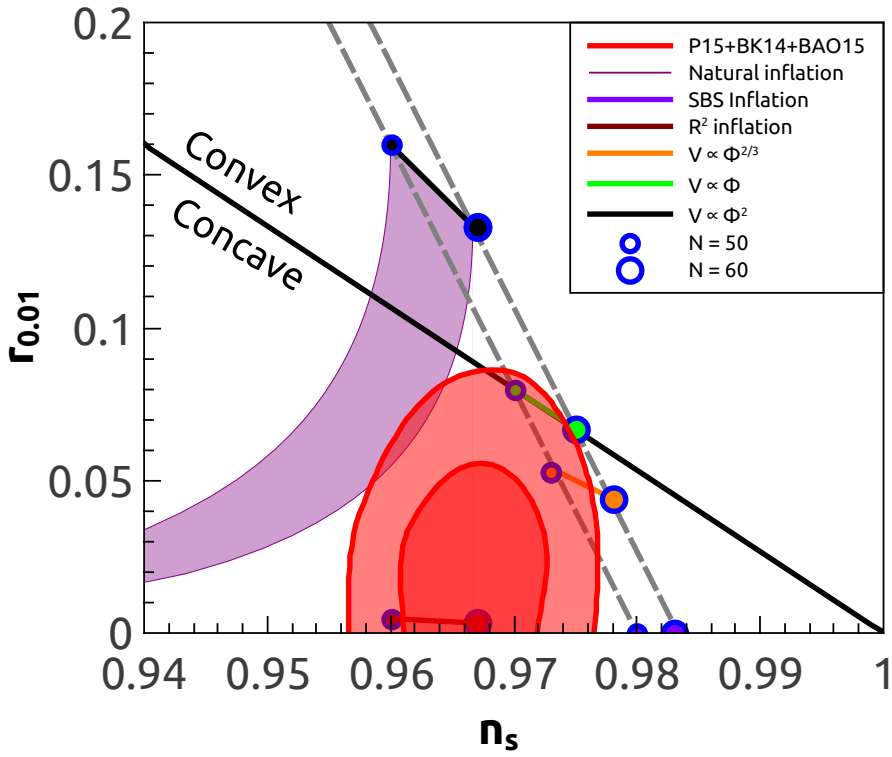


FIG. 4: Comparing the inflation models with the observational constraints.

model are

$$r = \frac{14n}{N}, \tag{25}$$

$$n_s = 1 - \frac{n+2}{2N}. \tag{26}$$

Here n is not necessarily an integer. Axion monodromy was supposed to achieve $V(\phi) \sim \phi^n$ inflation model in string theory. For example, $n = 2/5,\ 2/3$ in [29], $n = 1$ in [30], and the models with higher power in [31, 32]. For $50 < N < 60$, the predictions of $V(\phi) \sim \phi^n$ inflation model are illustrated in the region between two grey dashed lines in Fig. 4. Unfortunately, we see that this class of inflation models are marginally disfavored at around 95% C.L..

In the natural inflation model [33, 34], the effective one-dimensional potential is given by $V(\phi) = m^2 f^2 \left(1 + \cos(\phi/f)\right)$ where f denotes the decay constant. The natural inflation

predicts

$$r = \frac{8}{(f/M_p)^2}\frac{1+\cos\theta_N}{1-\cos\theta_N}, \tag{27}$$

$$n_s = 1-\frac{1}{(f/M_p)^2}\frac{3+\cos\theta_N}{1-\cos\theta_N}, \tag{28}$$

where

$$\cos\frac{\theta_N}{2} = \exp\left(-\frac{N}{2(f/M_p)^2}\right) . \tag{29}$$

For $50 < N < 60$, the different decay constant corresponds to different predictions. See the purple shaded region in Fig. 4. Compared to the constraints from data, the natural inflation model is also marginally disfavored at 95% C.L..

In the spontaneously broken SUSY (SBS) inflation model [35], the potential of inflaton field takes the form of $V(\phi) = V_0\left(1+c\ln\frac{\phi}{Q}\right)$ where V_0 is dominant and $c << 1$. This inflation model predicts

$$r \simeq 0, \tag{30}$$

$$n_s = 1-\frac{1}{N}. \tag{31}$$

It is also disfavored at more than 95% C.L., because it predicts a large scalar spectral index. If the soft SUSY breaking term is taken into account, the scalar spectral index can shift to fit the data [36, 37].

In the Starobinsky inflation model [1], the inflationary expansion of the Universe is driven by a higher derivative term in the action, namely $S = \frac{M_p^2}{2}\int d^4x\sqrt{-g}\left(R+\frac{R^2}{6M^2}\right)$ where M denotes an energy scale. The tensor-to-scalar ratio and the scalar spectral index in Starobinsky inflation model are given by

$$r \simeq \frac{12}{N^2}, \tag{32}$$

$$n_s = 1-\frac{2}{N}, \tag{33}$$

in [38, 39]. Even though this inflation model can fit the data quite well, why the terms with higher powers of R are all suppressed [40] is still an open question.

B. Constraints on typical inflation models

In this subsection, we propose a new method to explore the space of inflation models. Similar to [41], we parametrize the slow-roll parameter $\epsilon(N)$ in terms of e-folding number

N for the typical inflation model as follows

$$\epsilon(N) = \frac{c/2}{(N+\Delta N)^p}, \tag{34}$$

where $c(>0)$ and p are two constants, and

$$\Delta N = \left(\frac{c}{2}\right)^{1/p}. \tag{35}$$

Here we introduce ΔN to keep $N = 0$ at the end of inflation, namely $\epsilon(N = 0) = 1$. See some extended investigations in [42–45]. Now the tensor-to-scalar ratio reads

$$r = \frac{8c}{(N+\Delta N)^p}. \tag{36}$$

From Eq. (20), we obtain

$$\eta = \frac{c}{(N+\Delta N)^p} - \frac{p}{2(N+\Delta N)}, \tag{37}$$

and then

$$n_s = 1 - \frac{c}{(N+\Delta N)^p} - \frac{p}{N+\Delta N}. \tag{38}$$

Even though this parametrization can not cover all of the canonical single-field slow-roll inflation models, it can really cover many well-known inflation models.

• For the inflation model with $V(\phi) \sim \phi^n$, we have $p = 1$ and $c = n/2$.

• For the Starobinsky model, we have $p = 2$ and $c = 3/2$.

• For the brane inflation model [46] with $V(\phi) = V_0(1 - (\mu/\phi)^{d-2})$, we have $p = 2(d-1)/d$, where d is the number of transverse dimensions. For example, the D3-Brane inflation in the KKLMMT setup predicts $p = 5/3$ and $c \simeq 0$ [47].

Up to now the exact e-folding number corresponds to the pivot scale k_p is still unknown. Usually it is considered to be a number between 50 and 60. In this subsection, we take N as a free parameter. Adopting the flat priors for $c \in [0, 100]$, $p \in [0.5, 3]$ and $N \in [50, 60]$, globally fitting P15+BK14+BAO data combination and finally marginalizing over other free parameters in the base ΛCDM model and N, we obtain the constraints on the parameters c and p, namely

$$p = 2.07^{+0.32}_{-0.28} \quad (68\%\ \text{C.L.}), \tag{39}$$

$$c < 65.7 \quad (95\%\ \text{C.L.}). \tag{40}$$

See Fig. 5 as well. We see that the inflation model with a monomial potential corresponds to $p = 1$ which is disfavored at more than 95% C.L.. But both the Brane inflation model and the Starobinsky inflation model still fit the data quite well.

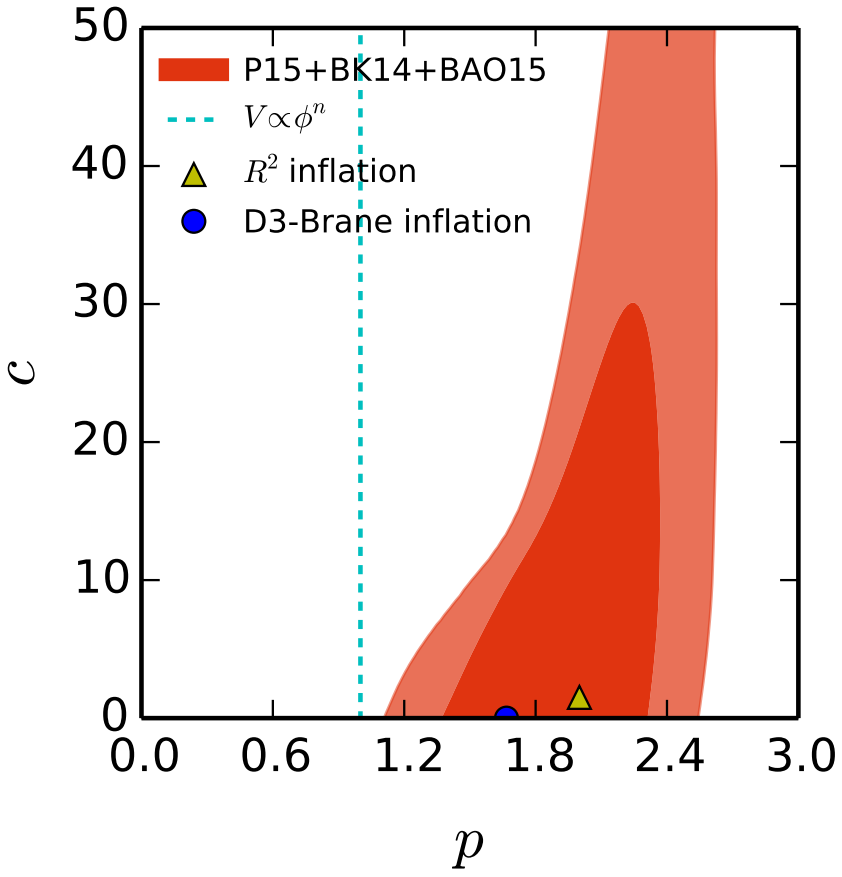


FIG. 5: Constraints on the space of inflation models from P15+BK14+BAO15.

IV. SUMMARY AND DISCUSSION

In this paper, we constrained the cosmological parameters in the base ΛCDM+r model and two extended models by jointly analyzing the data combination including *Planck* 2015 data of CMB anisotropies and polarizations as well as CMB lensing, BICEP2 & *Keck Array* data of B-mode polarization up to and including 2014 observing season, and the anisotropic BAO distance scales from SDSS-III BOSS DR12 together with the isotropic 6dFGS and MGS BAO data. Comparing with the predictions of inflation models, we find that the inflation model with a concave potential is preferred and both the inflation model with a monomial potential and the natural inflation model are marginally disfavored at 95% C.L.. But both the Brane inflation model and the Starobinsky inflation model still give a good fit to the current data.

Even though there is no evidence for supporting a non-zero running of scalar spectral index, a positive running of running in order of $\mathcal{O}(10^{-2})$ provides a slightly better fit to the data. Such a positive running of running can significantly relax the Lyth bound on the tensor-to-scalar ratio to 0.1 [48].

Before closing this paper, we also want to sketch the potential of inflaton field according to the current cosmological data. To summarize, the preferred inflation potential goes like that as follows

$$V(\phi) = \Lambda_* - \delta V(\phi), \tag{41}$$

where Λ_* is an effective cosmological constant which determines the energy scale of inflation, and the dynamics of inflation is described by the subdominant term $\delta V(\phi)$. Since the concave shape of potential is preferred, $\delta V''(\phi) > 0$. For example, for

$$V(\phi) = \Lambda_* \left[1 - \left(\frac{\phi}{\mu}\right)^n\right], \tag{42}$$

where μ is an energy scale, n is related to p in Eq. (34) by

$$n = \frac{2(p-1)}{p-2} \quad \text{for } p > 1 \text{ and } p \neq 2. \tag{43}$$

Note that $p = 2$ corresponds $V(\phi) = \Lambda_* [1 - \exp(-\phi/\mu)]$. From Sec. III B, we find $p > 1$ which implies $n < 0$ or $n > 2$ and the potential is certainly concave. Now we still cannot distinguish the sign of n. We hope that the accurate experiments will tell us more detail about inflation in the near future.

Acknowledgments We acknowledge the use of HPC Cluster of SKLTP/ITP-CAS. This work is supported by Top-Notch Young Talents Program of China and grants from NSFC (grant NO. 11322545, 11335012 and 11575271). QGH would also like to thank the participants of the advanced workshop "Dark Energy and Fundamental Theory" supported by the Special Fund for Theoretical Physics from the National Natural Science Foundations of China (grant No. 11447613) for useful conversation.

[1] A. A. Starobinsky, Phys. Lett. B **91**, 99 (1980).

[2] A. H. Guth, Phys. Rev. D **23**, 347 (1981).

[3] A. D. Linde, Phys. Lett. B **108**, 389 (1982).

[4] A. Albrecht and P. J. Steinhardt, Phys. Rev. Lett. **48**, 1220 (1982).

[5] R. Adam *et al.* [Planck Collaboration], arXiv:1502.01582 [astro-ph.CO].

[6] P. A. R. Ade *et al.* [Planck Collaboration], arXiv:1502.02114 [astro-ph.CO].

[7] P. A. R. Ade *et al.* [BICEP2 Collaboration], Phys. Rev. Lett. **112**, 241101 (2014) [arXiv:1403.3985 [astro-ph.CO]].

[8] M. J. Mortonson and U. Seljak, JCAP **1410**, 035 (2014) [arXiv:1405.5857 [astro-ph.CO]].

[9] R. Flauger, J. C. Hill and D. N. Spergel, JCAP **1408**, 039 (2014) [arXiv:1405.7351 [astro-ph.CO]].

[10] R. Adam *et al.* [Planck Collaboration], arXiv:1409.5738 [astro-ph.CO].

[11] C. Cheng, Q. G. Huang and S. Wang, JCAP **1412**, no. 12, 044 (2014) [arXiv:1409.7025 [astro-ph.CO]].

[12] P. A. R. Ade *et al.* [BICEP2 and Planck Collaborations], Phys. Rev. Lett. **114**, 101301 (2015) [arXiv:1502.00612 [astro-ph.CO]].

[13] P. A. R. Ade *et al.* [BICEP2 and Keck Array Collaborations], arXiv:1510.09217 [astro-ph.CO].

[14] A. J. Cuesta *et al.*, arXiv:1509.06371 [astro-ph.CO].

[15] H. Gil-Marin *et al.*, arXiv:1509.06373 [astro-ph.CO].

[16] F. Beutler *et al.*, Mon. Not. Roy. Astron. Soc. **416**, 3017 (2011) [arXiv:1106.3366 [astro-ph.CO]].

[17] A. J. Ross, L. Samushia, C. Howlett, W. J. Percival, A. Burden and M. Manera, Mon. Not. Roy. Astron. Soc. **449**, no. 1, 835 (2015) [arXiv:1409.3242 [astro-ph.CO]].

[18] A. R. Liddle and D. H. Lyth, Phys. Lett. B **291**, 391 (1992) [astro-ph/9208007].

[19] C. Cheng and Q. G. Huang, Eur. Phys. J. C **74**, no. 11, 3139 (2014) [arXiv:1403.7173 [astro-ph.CO]].

[20] Q. G. Huang and S. Wang, JCAP **1506**, no. 06, 021 (2015) [arXiv:1502.02541 [astro-ph.CO]].

[21] G. Cabass, L. Pagano, L. Salvati, M. Gerbino, E. Giusarma and A. Melchiorri, arXiv:1511.05146 [astro-ph.CO].

[22] Q. G. Huang, S. Wang and W. Zhao, JCAP **1510**, no. 10, 035 (2015) [arXiv:1509.02676 [astro-ph.CO]].

[23] A. Lewis, A. Challinor and A. Lasenby, Astrophys. J. **538**, 473 (2000) [astro-ph/9911177].

[24] C. Howlett, A. Lewis, A. Hall, and A. Challinor, JCAP **04**, 027 (2012).

[25] A. Lewis and S. Bridle, Phys. Rev. D **66**, 103511 (2002) [astro-ph/0205436].

[26] Q. G. Huang, Sci. China Phys. Mech. Astron. **58**, no. 11, 110401 (2015) [arXiv:1407.4639 [astro-ph.CO]].

[27] J. Martin, C. Ringeval and V. Vennin, Phys. Dark Univ. **5-6**, 75 (2014) [arXiv:1303.3787 [astro-ph.CO]].

[28] A. D. Linde, Phys. Lett. B **129**, 177 (1983).

[29] E. Silverstein and A. Westphal, Phys. Rev. D **78**, 106003 (2008) [arXiv:0803.3085 [hep-th]].

[30] L. McAllister, E. Silverstein and A. Westphal, Phys. Rev. D **82**, 046003 (2010) [arXiv:0808.0706 [hep-th]].

[31] F. Marchesano, G. Shiu and A. M. Uranga, JHEP **1409**, 184 (2014) [arXiv:1404.3040 [hep-th]].

[32] L. McAllister, E. Silverstein, A. Westphal and T. Wrase, JHEP **1409**, 123 (2014) [arXiv:1405.3652 [hep-th]].

[33] K. Freese, J. A. Frieman and A. V. Olinto, Phys. Rev. Lett. **65**, 3233 (1990).

[34] F. C. Adams, J. R. Bond, K. Freese, J. A. Frieman and A. V. Olinto, Phys. Rev. D **47**, 426 (1993) [hep-ph/9207245].

[35] G. R. Dvali, Q. Shafi and R. K. Schaefer, Phys. Rev. Lett. **73**, 1886 (1994) [hep-ph/9406319]; E. J. Copeland, A. R. Liddle, D. H. Lyth, E. D. Stewart and D. Wands, Phys. Rev. D **49**, 6410 (1994); P. Binetruy and G. R. Dvali, Phys. Lett. B **388**, 241 (1996) [hep-ph/9606342]; E. D. Stewart, Phys. Rev. D **51**, 6847 (1995) [hep-ph/9405389]; D. H. Lyth and A. Riotto, Phys. Rept. **314**, 1 (1999) [hep-ph/9807278].

[36] M. U. Rehman, Q. Shafi and J. R. Wickman, Phys. Lett. B **683**, 191 (2010) [arXiv:0908.3896 [hep-ph]].

[37] C. Pallis and Q. Shafi, Phys. Lett. B **725**, 327 (2013) [arXiv:1304.5202 [hep-ph]].

[38] V. F. Mukhanov and G. V. Chibisov, JETP Lett. **33**, 532 (1981) [Pisma Zh. Eksp. Teor. Fiz. **33**, 549 (1981)].

[39] A. A. Starobinsky, Sov. Astron. Lett. **9**, 302 (1983).

[40] Q. G. Huang, JCAP **1402**, 035 (2014) [arXiv:1309.3514 [hep-th]].

[41] Q. G. Huang, Phys. Rev. D **76**, 061303 (2007) [arXiv:0706.2215 [hep-th]].

[42] V. Mukhanov, Eur. Phys. J. C **73**, 2486 (2013) [arXiv:1303.3925 [astro-ph.CO]].

[43] D. Roest, JCAP **1401**, 007 (2014) [arXiv:1309.1285 [hep-th]].

[44] J. Garcia-Bellido, D. Roest, M. Scalisi and I. Zavala, Phys. Rev. D **90**, no. 12, 123539 (2014) [arXiv:1408.6839 [hep-th]].

[45] R. Gobbetti, E. Pajer and D. Roest, JCAP **1509**, no. 09, 058 (2015) [arXiv:1505.00968 [astro-ph.CO]].

[46] G. R. Dvali and S. H. H. Tye, Phys. Lett. B **450**, 72 (1999) [hep-ph/9812483].

[47] S. Kachru, R. Kallosh, A. D. Linde, J. M. Maldacena, L. P. McAllister and S. P. Trivedi, JCAP **0310**, 013 (2003) [hep-th/0308055].

[48] Q. G. Huang, Phys. Rev. D **91**, no. 12, 123532 (2015) [arXiv:1503.04513 [astro-ph.CO]].